Journal of Computer-Aided Molecular Design (2017) 31:1053–1062
https://doi.org/10.1007/s10822-017-0086-6

Discovery of small molecules binding to the normal conformation of prion by combining virtual screening and multiple biological activity evaluation methods

Lanlan Li[1] · Wei Wei[2] · Wen-Juan Jia[3] · Yongchang Zhu[2] · Yan Zhang[1,2] · Jiang-Huai Chen[3] · Jiaqi Tian[2] · Huanxiang Liu[2] · Yong-Xing He[3] · Xiaojun Yao[1,4]

Received: 24 April 2017 / Accepted: 15 November 2017 / Published online: 20 November 2017

Abstract

Conformational conversion of the normal cellular prion protein, PrP^{C}, into the misfolded isoform, PrP^{Sc}, is considered to be a central event in the development of fatal neurodegenerative diseases. Stabilization of prion protein at the normal cellular form (PrP^{C}) with small molecules is a rational and efficient strategy for treatment of prion related diseases. However, few compounds have been identified as potent prion inhibitors by binding to the normal conformation of prion. In this work, to rational screening of inhibitors capable of stabilizing cellular form of prion protein, multiple approaches combining docking-based virtual screening, steady-state fluorescence quenching, surface plasmon resonance and thioflavin T fluorescence assay were used to discover new compounds interrupting PrP^{C} to PrP^{Sc} conversion. Compound **3253-0207** that can bind to PrP^{C} with micromolar affinity and inhibit prion fibrillation was identified from small molecule databases. Molecular dynamics simulation indicated that compound **3253-0207** can bind to the hotspot residues in the binding pocket composed by β1, β2 and α2, which are significant structure moieties in conversion from PrP^{C} to PrP^{Sc}.

Keywords Prion · Virtual screening · Fluorescence quenching · Fibrillation · Surface plasmon resonance · Molecular dynamics simulation

Introduction

Transmissible spongiform encephalopathies (TSEs), also known as prion diseases, affect human and a variety of mammalian species. These diseases are progressive, degenerative disorders of the central nervous system that result in dementia, significant motor dysfunction, and ultimately lead to death [1]. The sporadic Creztzfeldt–Jakob disease (CJD) is the most common form of prion disease in human, affecting about 2 persons per million annually worldwide. CJD has symptoms of rapidly progressing dementia with a median survival of 4–6 months [2].

Prion diseases are mainly caused by misfolding and aggregation of endogenously expressed proteins [3–5]. The endogenous, properly folded form is denoted as PrP^{C}, whereas the disease-linked, misfolded form is denoted as PrP^{Sc}. Though share identical primary structure, the two forms of prion protein displayed distinct properties. PrP^{C} is an extracellular membrane anchored protein that contains a flexible, unstructured N-terminal domain and a globular C-terminal domain comprising two short antiparallel β

Electronic supplementary material The online version of this article (https://doi.org/10.1007/s10822-017-0086-6) contains supplementary material, which is available to authorized users.

✉ Huanxiang Liu
hxliu@lzu.edu.cn

✉ Yong-Xing He
heyx@lzu.edu.cn

✉ Xiaojun Yao
xjyao@lzu.edu.cn

[1] State Key Laboratory of Applied Organic Chemistry and Department of Chemistry, Lanzhou University, Lanzhou 730000, People's Republic of China

[2] School of Pharmacy, Lanzhou University, Lanzhou 730000, People's Republic of China

[3] School of Life Sciences, Lanzhou University, Lanzhou 730000, People's Republic of China

[4] State Key Laboratory of Quality Research in Chinese Medicine, Macau Institute for Applied Research in Medicine and Health, Macau University of Science and Technology, Taipa, Macau, People's Republic of China

strands and three α helices. The PrP^{Sc} form is polymeric and enriched in β sheets and also possesses certain aberrantly physiochemical properties such as insolubility, protease resistance and the capability to aggregate into amyloid-like fibrils [6, 7]. Although conversion of PrP^{C} into PrP^{Sc} is linked with prion pathogenesis and the mechanism of PrP^{Sc} formation is still not well understood [8, 9]. Conformational conversion of PrP^{C} to PrP^{Sc} is conventionally considered as a central event for the onset of prion diseases [4, 10].

To date, numerous studies have been carried out to develop therapeutics targeting prion diseases by using prion-infected cell lines. A number of compounds including pentosan polysulfate, dextran sulfate, Congo red, suramin, HPA-23, dendritic polyamines and quinacrine were identified that can reduce the level of PrP^{Sc} in cell culture [11–13]. However, most of these have been shown to be ineffective against a variety of prion strains in animal models. The current anti-prion compounds were investigated mostly by screening known bioactive compounds [13]. The detailed molecular target and mechanism of action of these active compounds remain unknown. Since most anti-prion compounds active in prion-infected cell lines have failed in vivo, more effective and rational drug discovery strategy is still urgent needed to rapidly screen large small molecule libraries.

Though it is still not clear how PrP^{C} is transformed into PrP^{Sc}, several hypotheses were proposed on the mechanism of PrP^{C} to PrP^{Sc} conversion. One of the widely accepted hypotheses is that PrP^{Sc} acts as a template for PrP^{C} to promote the pathogenesis conversion and this conversion involves only conformational change [3, 4, 14, 15]. Based on this hypothesis, three main strategies can be adopted for treatment of prion diseases, (i) stabilization of PrP^{C} conformation; (ii) clearance of PrP^{Sc} form and (iii) inhibition of conversion from PrP^{C} to PrP^{Sc} [12, 16–18]. Stabilization of the normal conformation with small molecules was demonstrated to be more attractive because conversion to PrP^{Sc} might be interrupted once the PrP^{C} conformation is stabilized [19, 20].

To discover small molecules that can stabilize PrP^{C} conformation, molecular docking-based virtual screening combined with steady-state fluorescence quenching, surface plasmon resonance (SPR) and thioflavin T (ThT) fluorescence based assay were used. Virtual screening has been widely used to screen large libraries of compounds and to identify those structures likely to bind to a drug target [21, 22]. In the present work, molecular docking based virtual screening was used to screen millions of compounds that can bind to normal conformation of prion. Steady-state fluorescence quenching method was applied to quickly study the interaction between the screened hits and prion [23, 24]. SPR method was further used to monitor the interaction between prion and small molecules because this method has been successfully used to binding affinity evaluation [25–28]. A fluorimetric ThT assay was used to follow the progress of amyloid fibril formation [29]. Molecular dynamics simulation [30] was further carried out to investigate the detailed dynamic interaction features between the potential binders and prion protein because MD simulation were effective tools to study the dynamic ligand–protein interaction mechanisms [31–33]. Compound **3253-0207** was proved to be able to bind to prion protein and could potentially stabilize the cellular PrP^{C} conformation and further inhibits fibrillation of prion protein.

Materials and methods

Virtual screening of small molecules binding to the normal conformation of prion

The whole virtual screening workflow was completed in the Schrodinger 2015 package. The mouse prion protein other than human prion protein was used in this study due to following reasons: mouse prion and human prion have quite high homology and the 3D structures overlapped well with a sequence identity of 91%; many previous works were also performed based on mouse prion protein; the binding site in the mouse prion protein was clearly defined while that of human prion is still unclear; there is no available human prion complexed with small molecules at present. The only available X-ray structure of small molecule and mouse prion complex (1.97 Å) has a better resolution. The crystal structure of mouse prion bound with promazine was obtained from Protein Data Bank (PDB code: 4MA7 [19]) for this study. The protein was protonated with pH of 7.0. The complex was minimized using OPLS2005 force field [34]. The docking grid file was generated based on the cocrystallized ligand using the Receptor Grid Generation module [35] with an enclosing box similar to the cocrystallized ligand. Multiple tautomers and protonation states were enumerated in the Ligand Preparation wizard for ~ 1.6 million small molecules in Chemdiv and Specs database. All ligands were initially optimized with the MMFFs force field and were pre-filtered using Lipinski's Rule of Five before virtual screening. All the remaining parameters were kept as default settings [36]. Prime MM–GBSA was applied to further evaluate the binding affinity. The docked binding modes were ranked according to the docking score and the predicted binding free energy. The final candidates for experiment validation were then manually selected according to their binding modes.

Cloning, expression and purification of moPrP(117–231)

The genes of PrP117–231 region containing 6×His tag was synthesized by GENEWIZ, Inc. (Suzhou, China) and was

cloned into the pET-28b derived vector (Novagen). The plasmid was transformed into *Escherichia coli* strain BL21(DE3) competent cells by heat-shock at 42 °C for 60 s. The cells were grown in Luria–Bertani (LB) medium containing 50 μg/ml kanamycin at 37 °C, 220 rpm to reach an OD_{600} between 0.6 and 1.0. Then 0.2 mM isopropyl β-D-1-thiogalactopyranoside (IPTG) was added to induce the PrP(117–231) expression at 16 °C, 220 rpm. About 20 h later, the cells were harvested by centrifugation. The inclusion bodies were sonicated, pelleted by centrifugation and extensively washed with washing buffer (20 mM Tris–HCl, pH 8.0, 150 mM NaCl, 0.5% Triton-X 100). The inclusion bodies were incubated with denaturing buffer containing 8 M urea (10 mM Tris–HCl, 100 mM NaH_2PO_4, 5 mM reduced glutathione, pH 8.0) in room temperature for 1 h with constant stirring. The denatured PrP was purified using metal affinity chromatography by loading onto a Ni–NTA agarose column. Removal of contaminants and refolding of prion protein were achieved with buffers plus a gradient of 8–0 M urea (10 mM Tris–HCl, 100 mM NaH_2PO_4, 5 mM reduced glutathione, pH 8.0) according to the references [19, 37, 38]. The nonspecifically bound impurities were removed by washing buffer (10 mM Tris–HCl, 100 mM NaH_2PO_4, 50 mM imidazole, pH 8.0) after the refolding. Finally, the pure his-tagged prion protein was eluted with an elution buffer (10 mM Tris–HCl, 100 mM NaH_2PO_4, 400 mM imidazole at pH 5.8). The purified protein was exchanged into storage buffer containing 10 mM Tris–HCl, 100 mM NaH_2PO_4 at pH 5.8 using ultra centrifugal filters (3 kDa molecular weight cutoff; Millipore). A 12% SDS-PAGE and the Bradford [39] method were used to determine the purity and the concentration.

Steady-state fluorescence quenching analysis

A Thermal Scientific™ Varioskan™ Flash multimode plate reader and a Perkin-Elmer LS 55 fluorescence spectrometer were used to record the fluorescence emission spectra. The Thermal Scientific plate reader was used to screen small molecules with a concentration of 100 μM. Those small molecules having larger fluorescence quenching ability were selected to measure fluorescence quenching with different concentrations. In all measurements, an excitation wavelength of 280 nm was adopted and the scan range was 285–430 nm. Prior to collecting the fluorescence spectra, the protein was diluted with storage buffer (10 mM Tris–HCl, 100 mM NaH_2PO_4, pH 5.8) to a final concentration of 10 μM and incubated with different concentrations for 15 min with shaking (220 rpm, 37 °C). The apparent binding constant was predicted using data from these fluorescence experiments according to the Stern–Volmer Eq. (1) [23, 40, 41]:

$$F_0/F = 1 + K_A[C] \tag{1}$$

where K_A is the formation constant of the complex, [C] is the concentration of the compound (quencher) in the titration. F_0 and F are the fluorescence value of the protein system in the absence and presence of a quencher.

Surface plasmon resonance assay

SPR experiments were carried out based on a Biacore X100 (GE Healthcare) equipped with a CM5 (research grade) sensor chip at 25 °C. The prion protein (117–231) was covalently immobilized onto the sensor surface at ~3000 response units (RUs) through a standard amine-coupling procedure in 10 mM sodium acetate (pH 5.5). In the binding experiments, PBS buffer supplied with 0.05% (v/v) surfactant P20 and 5% (v/v) DMSO (Sigma-Aldrich) was used as running buffer. Before it was used in the instrument, the running buffer was degassed for about 5 min. The small molecules were dissolved in DMSO and a calibration procedure was included to eliminate variations in the bulk responses between samples caused by the presence of high refractive index DMSO [42, 43]. The compounds were diluted with PBS buffer and injected for 60 s in contact phase followed by 60 s in dissociation phase with a flow rate of 30 μl/min in the binding analysis. All the response levels obtained during the analysis were corrected according to the DMSO calibration plot. For binding response of compounds, a single-site interaction model was applied. This approach leads to a unique K_D which corresponds to the higher affinity site constant:

$$R_{eq} = \frac{R_{max} \times [L]}{K_D + [L]} \tag{2}$$

where R_{eq} is the SPR response at equilibrium; R_{max} is the maximum capacity of the ligand for the analytes; [L] is the analyte concentration and K_D is the dissociation constant. The obtained sensor grams were processed and analyzed using Biacore X100 Evaluation software (GE Healthcare).

In vitro amyloid fibrils formation inhibition assay

PrP(117–231) was converted to fibril form in vitro based on reported methods with minor modification [44, 45]. The prion protein was diluted to 20 μM with solution buffer of 10 mM Tris–HCl, 100 mM NaH_2PO_4, pH 5.8 and incubated with continuous shaking at 220 rpm, 37 °C. After incubation for several hours, 100 μl aliquots of the incubation solution were withdrawn to monitor protein fibril formation. To determine inhibition ability of fibril formation, various concentrations of the positive compounds were co-incubated with the fibril formation systems. A specific thioflavin T (ThT) dye was used to monitor the kinetics of fibril formation. The ThT stock solution was prepared as 400 μM and then diluted to 20 μM before measuring the fluorescence.

20 μM ThT solution was mixed with 100 μl incubated fibril formation aliquot to make both the ThT and prion protein work concentration as 10 μM. The fluorescence spectrum was recorded with excitation at 440 nm and maximum emission at 485 nm. To quantitatively describe prion fibrillation inhibition, the small molecules at different concentrations was incubated with prion. After 48 h, the co-incubation samples were subjected to SDS-PAGE method to detect prion monomers.

Molecular dynamics simulation

MD simulation was carried out using the Amber 12 software package [46]. The ligand-prion protein complex was obtained by molecular docking. Gaussian 09 program [47] was used to perform geometry optimization and to calculate electrostatic potential of the ligand by using the Hartree–Fock method with 6-31G* basis set. To describe the partial atomic charges, the antechamber module of AMBER was used to generate the restrained electrostatic potential (RESP) [48, 49]. The parameters of the ligand and protein were described adopting the general AMBER force field (GAFF) [50] and the standard AMBER force field (ff99SB) [51], respectively. MD simulations were performed on the prion protein with and without ligand, at the temperature of 310 K for 125 ns using the TIP3P water in an octahedron box with 12 Å around the biomolecules.

Binding free energy calculation by MM–GBSA method

The binding free energy of **3253-0207** to prion protein was analyzed by molecular mechanics generalized born surface area (MM–GBSA) [52–54] method, integrated in the Amber 12 package. The first step of MM–GBSA is to generate multiple snapshots from the stable MD production trajectory of the complex. Here, 1000 snapshots were extracted from last 25 ns of MD trajectory, equally spaced at 5 ps intervals. For each snapshot, a free energy is calculated for each molecular species (complex, receptor, and ligand), and the ligand binding free energy is estimated as follows:

$$\Delta G_{bind} = G_{complex} - G_{receptor} - G_{ligand} \quad (3)$$

where $G_{complex}$, $G_{receptor}$, and G_{ligand} are the free energy of complex, receptor, and ligand molecules, respectively. The free energy (G_{bind}) was calculated based on an average over the extracted snapshots. Each state is estimated from the molecular mechanics energy E_{gas}, the solvation free energy G_{sol}, and the solute entropy S, respectively.

$$G_{bind} = E_{gas} + G_{sol} - TS \quad (4)$$

$$E_{gas} = E_{int} + E_{vdW} + E_{ele} \quad (5)$$

$$G_{sol} = G_{GB} + G_{sol-np,GB} \quad (6)$$

$$G_{sol-np,GB} = \gamma SASA \quad (7)$$

where E_{gas} is the gas-phase energy; E_{int} is the internal energy; E_{ele} and E_{vdW} are the Coulomb and van der Waals energies. G_{sol} is the solvation free energy and can be decomposed into polar and nonpolar contributions. G_{GB} is the polar solvation contribution calculated by solving the GB equation. Dielectric constants for solute and solvent were set to 1 and 80, respectively. G_{sol-np} is the nonpolar solvation contribution and was estimated by the SASA determined using a water probe radius of 1.4 Å. The surface tension constant γ was set to 0.0072 kcal/(mol Å^2) [55]. T and S are the temperature and the total solute entropy, respectively. Vibrational entropy contributions can be estimated by statistical thermodynamics, using normal-mode analysis [56]. As our aim is not to obtain the absolute Gibbs energy but to analyze the interaction features, the entropy contribution was not included.

Results and discussion

The results of virtual screening

In the present work, virtual screening workflow was performed to screen potential compounds stabilizing the antiparallel β strands. Before the virtual screening workflow, the accuracy of docking protocol was checked by redocking the ligand promazine into the prion. The comparison of the crystalized ligand and docked ligand conformation is shown in Fig. 1. As can be seen, the ligand was docked into a hydrophobic pocket composed of residues from helix α2 and anti-parallel β-strands. The rmsd between the crystal and the docked pose was 1.5 Å and the main tricyclic skeletons in the two ligands were aligned very well. The ligand had a docking score of − 5.00 kcal/mol and predicted binding free energy of − 44.78 kcal/mol.

After verification of docking protocol, virtual screening workflow was carried out against ~ 1.6 million compounds, using the standard VS protocol with the HTVS, SP and XP screening steps. In each step, 10% compounds were kept for the next step processing. The final compounds were further processed using the Prime MM–GBSA method to predict the binding free energy. Based on the docking score and predicted binding free energy, those compounds with docking score and binding energy higher than that of the redocked ligand were removed. Furthermore, clustering analysis was performed to eliminate redundancy and enable structural diversity. Compounds forming favorable

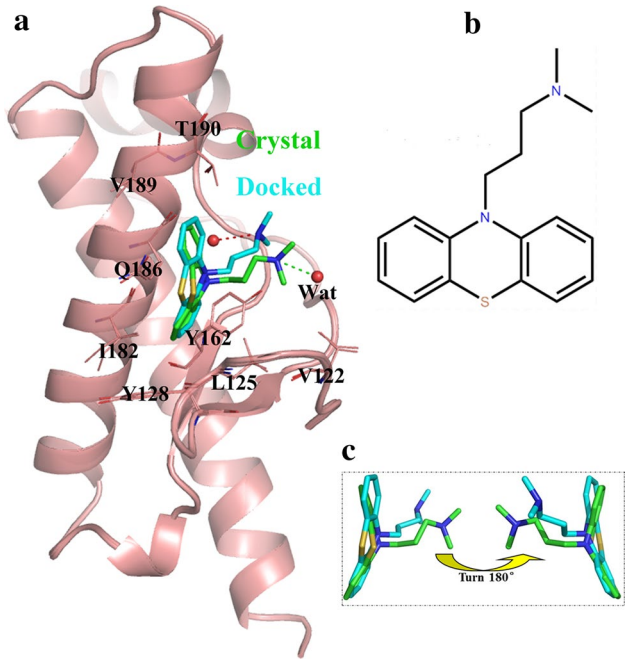

Fig. 1 The structure of prion protein complexed with promazine. **a** Comparison of the computational docking of promazine (carbons in cyan) in the prion binding pocket versus the reported crystal structure. Water molecules involved in hydrogen bond interaction were shown in small red spheres. **b** Structure of promazine. **c** Poses of promazine in the binding pocket

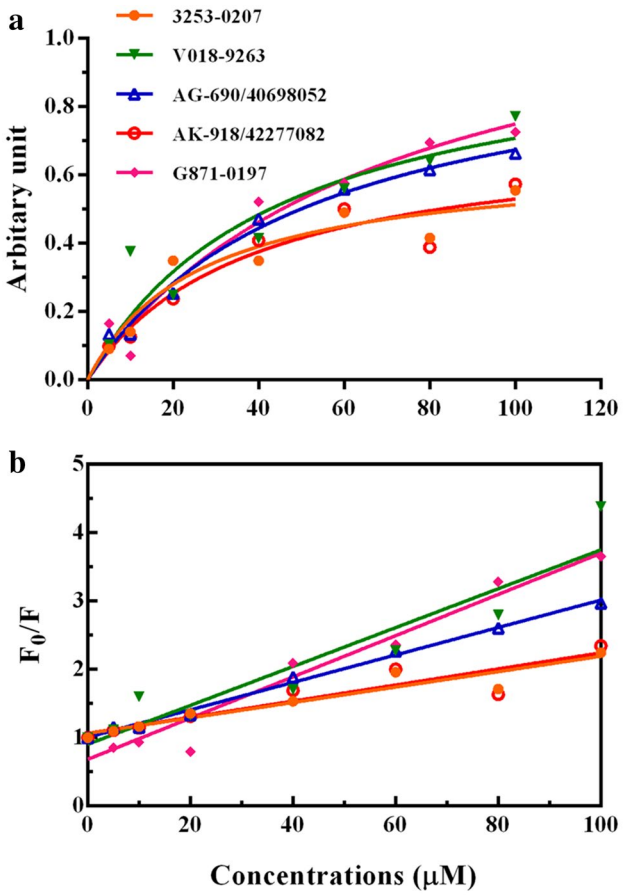

Fig. 2 Quenching of prion protein by five compounds, **3253-0207** (orange solid circles), V018-9263 (green solid triangles), AG-690/40698052 (blue hollow triangles), AK-918/42277082 (red hollow circles) and G871-0197 (magenta solid diamonds). **a** Concentration dependent fluorescence quenching fitted to one site specific binding model (Y-axis represents the relative fluorescence quenching which defined as $(F_0-F)/F_0$). **b** Linear Stern–Volmer plot

interaction with prion protein were selected manually by inspecting interactions between the protein and ligands. 121 compounds were selected and purchased for further biological assays.

Identification of compounds interacting with PrP by using fluorescence titration assay

The global region of prion protein was over-expressed in *E. coli* and purified for the protein–ligand binding experiments. The maximum excitation and emission wavelengths of the purified prion protein (10 μM) were determined as 280 and 345 nm, respectively. Firstly, the fluorescence quenching ability of 121 compounds on prion protein was evaluated at a concentration of 100 μM, using a single point scan mode at excitation of 280 nm and emission of 345 nm. According to the fluorescence quenching assay, 14 hits among the 121 compounds had a quenching ability larger than 50% and were selected for further test. The quenching abilities were averaged by three independent fluorescence values and ranged from 51.4 to 78.2% (Table S1). The cocrystallized promazine gave a quenching ability of (16.5 ± 0.28)%.

Subsequently, 14 hits were further tested to investigate concentration dependent fluorescence quenching profiles. Only 5 compounds demonstrated well correlation between concentrations and quenching abilities (Fig. 2). The cocrystallized promazine failed to quench prion fluorescence in concentration dependent manner. At the same time, the excluded 9 molecules were checked whether they are promiscuous compounds using the PAINS-Remover (http://cbligand.org/PAINS/search_struct.php) and only one molecule (3284-1064) was filtered out for containing a "2-hydroxyphenyl-hydrazone" moiety which was reactive as recorded in the reference [57]. Subsequently, the concentration dependent fluorescence quenching of the other 5 compounds was fitted to one site specific binding model using the GraphPad Prism 6 software (Fig. 2a). The strong quenching of the fluorescence suggests that the conformation of aromatic residue around the compound binding pocket were changed due to the binding of tested compounds. The K_d values of the 5 hits were calculated according to Eq. (1) and were presented in Table S1. The 5 compounds interacted with

prion with K_d values ranging from 26 to 71 μM. Compound **3253-0207** interacted with prion protein and gave the lowest K_d of 26.23 μM. The intensity of fluorescence quenching of 5 compounds was quantified using Stern–Volmer plot (Fig. 2b). The obtained Stern–Volmer plot from the fluorescence measurement is presented as linear lines.

Study of the prion-small molecule interaction by SPR based binding assay

Since there may occur false positives in the fluorescence quenching experiments, it is necessary to further confirm binding affinities of the compounds identified by fluorescence assay. Surface plasmon resonance (SPR) is an excellent approach which can measure binding affinities between various binding systems. Therefore, 5 hit compounds were further tested using SPR to observe their binding ability to PrP^C. Before carrying out the binding analysis, a calibration was performed to eliminate the bulky refractive influence of solvent by using different DMSO concentrations ranging from 4.5 to 5.8% (V/V) (Fig. S1a). After solvent correction, 100 μM compounds were loaded at the same time to verify reliability of the results. As shown in Fig. S1a, the binding response of samples located in a region distinguished by two vertical lines, which were close to each other, indicating a fine quality of solvent correction. Meanwhile, the binding abilities were analyzed at a concentration of 100 μM (Fig. S1b). SPR results proved that the majority of the compounds interacted with PrP^C. Among the 5 compounds, **3253-0207** interacted with prion protein with an equilibrium binding response of about 80 RUs, which was greater than that of the other compounds (Fig. S1b). It is worth mentioning that binding response of AK-918/42277082 got a negative value after solvent calibration indicating low binding affinity to prion protein. Promazine was a weak binder of prion with a binding response of 12.6 RUs.

Based on the binding analysis results, the apparent affinities of **3253-0207** with mPrP(117–231) was further determined. A wide range of half-diluted **3253-0207** concentrations were guided over the sensor chip surface, ranging from 3.125 to 100 μM. The binding responses were recorded as sensor grams (Fig. 3a). As indicated in Fig. 3a, both the association and dissociation phases were rapid which obeyed the fast-on and fast-off interaction pattern. A single-site model (Eq. 2) was used to fit the obtained equilibrium binding responses versus ligand concentrations. The calculated value of K_D was 2.603×10^{-5} M, which was in good agreement with that obtained from fluorescence assay. The data confirmed the good binding affinity of **3253-0207** to mPrP(117–231).

The inhibition of prion amyloid fibrils formation by compound 3253-0207

To determine the inhibition effect of **3253-0207** on prion aggregation, prion with and without compound **3253-0207** were incubated. The monomers were detected with native SDS-PAGE after incubation. As displayed in Fig. 4a, after fibril conversion for 48 h, there were little monomers in PrP without compound **3253-0207**. When **3253-0207** was added, the quantities of prion monomers increased as the ligand concentration increased. Therefore, compound **3253-0207** could stabilize the PrP^C form which would help to interrupt prion aggregation process.

The enhanced fluorescence emission of the dye ThT was frequently used for monitoring the kinetics of amyloid fibril

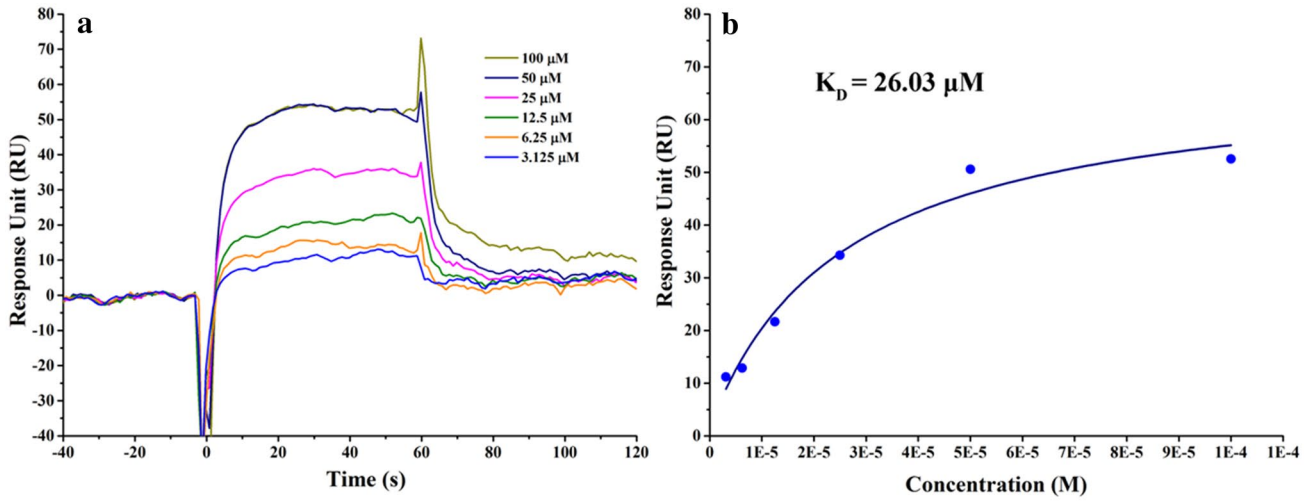

Fig. 3 Binding affinity analysis of **3253-0207**. **a** Overlay of sensorgrams for **3253-0207** binding to mPrP(117–231), obtained using different concentrations: 3.125, 6.25, 12.5, 25, 50 and 100 μM. **b** Response data at equilibrium versus **3253-0207** concentration

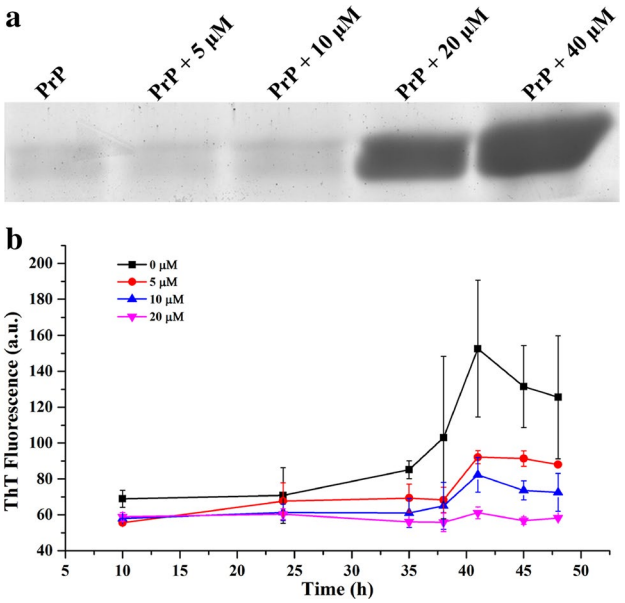

Fig. 4 Compound **3253-0207** could inhibit prion fibril formation. **a** Compound **3253-0207** could stabilize prion monomers as detected using native SDS-PAGE. **b** Effect of **3253-0207** on prion fibril formation kinetics as monitored by ThT fluorescence. The data were obtained at excitation of 440 nm and emission of 485 nm, averaged by a triplicate experiment with error bars indicated

formation [58–60]. In this study, the effects of compound **3253-0207** on fibril formation kinetics of the recombinant mouse PrP were detected using the ThT binding assay, as a function of compound concentrations (Fig. 4b). As can be seen, prion protein without any inhibitor aggregated into fibril form after ~30 h as reflected in an increase of ThT fluorescence. The amyloid formation was inhibited when 5 μM compound **3253-0207** was co-incubated (red line with round circles), accompanied by a remarkable decline of the maximum ThT intensity (Fig. 4b). As indicated in Fig. 4b, fibril formation was totally inhibited by compound **3253-0207** at 20 μM (magenta line with inverted triangles) on the investigated timescale. SDS-PAGE and ThT assay results proved that compound **3253-0207** could stabilize prion protein and inhibit prion aggregation.

Molecular dynamics simulation of the complex of prion and compound 3253-0207

To further explore the binding mechanism and provide more information for future drug design, 125 ns molecular dynamics simulation was performed for prion protein with or without compound **3253-0207**. To monitor the convergence of simulation, the evolutions of root-mean-square deviation (RMSD) value versus time were extracted from the trajectories (Fig. 5). As can be seen from the backbone RMSD (red line in Fig. 5), the complex system showed small RMSD with less

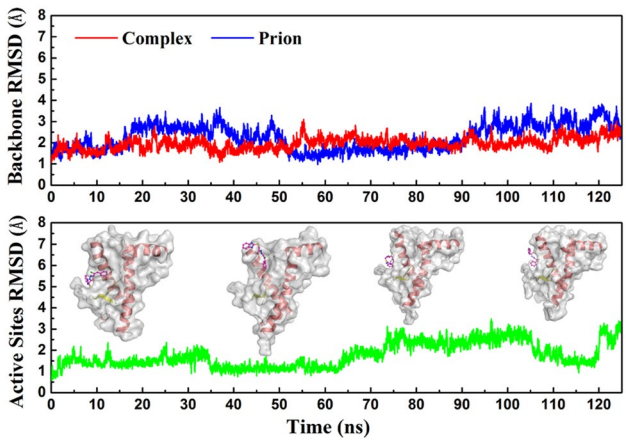

Fig. 5 The evolutions of RMSD value versus the simulation time

fluctuations, while the blank prion protein system (blue line in Fig. 5) fluctuated largely at the beginning and reached equilibrium after about 90 ns. The active sites residues around 5 Å of the ligand were much flexible during the simulation (green line in Fig. 5). Along the whole simulation, the ligand changed its conformation to form more stable complex (cartoon and sticks representation in Fig. 5) which caused fluctuation and retained equilibrium pose finally (cyan sticks in Fig. S2). The distances of ligand to H2 (residues 171–194) and H3 (residues 200–226) further proved the conformation change of ligand in the binding pocket (Fig. S2). As the initial complex structure was obtained using molecular docking, the binding pose was not stable enough at the beginning. After 60 ns of simulation, the benzimidazole moiety flipped towards C-terminal of H2. The RMSF of residues were displayed in Fig. 6. As can be seen, binding of the compound **3253-0207** make two regions

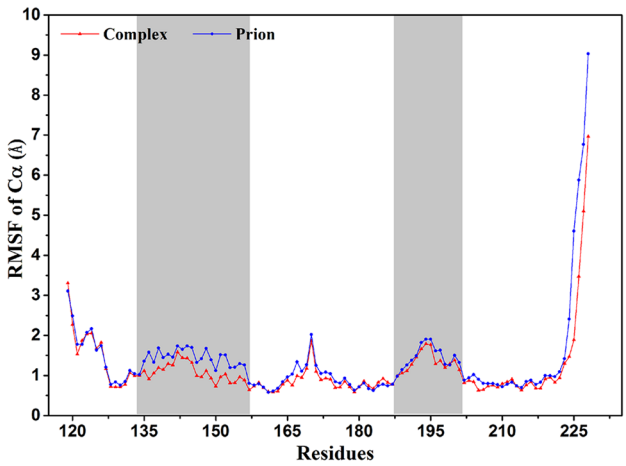

Fig. 6 RMSF of the two systems along the simulations. The RMSFs of complex are in red and the RMSFs of apo-protein are in blue. Regions with gray background indicate obvious disparity of the two systems

helix-1 and the C-terminal of helix-2 of the complex became more stable.

To investigate the stabilization mechanism, the secondary structure evolution were analyzed and displayed in Fig. S3 and Table S2. As can be seen, when bound with the ligand, helix-3 of the protein maintained more helical structure than the apo protein, which was also indicated in the helix contents with (55.52 ± 0.15)% in complex and (52.10 ± 0.24)% in apo protein. The average content of β-sheet in complex was lower than in apo protein (4.99% in complex, 6.89% in apo protein). Moreover, residues 117–130 in the complex system had more regular structures than in the system without the ligand, which is important for prion protein to keep the normal cellular form (PrP^C).

The binding free energy between **3253-0207** and prion protein was obtained from the MM–GBSA calculation (Table 1). **3253-0207** bound to PrP with a binding energy of −22.59 kcal/mol. The negative non-polar energy $\Delta G_{nonpolar}$ (−31.33 kcal/mol) mainly composed of Van der Waals was the driving force of the complex formation. Nonpolar solvation terms (ΔG_{sol-np}, −4.35 kcal/mol) contribute slightly favorably to the binding. The polar interaction contributed unfavorably to the binding of ligand. The intermolecular electrostatic interactions (ΔE_{ele}) had favorable contribution to binding process, while they were compensated by the large desolvation penalties ($\Delta G_{sol-ele}$) (Table 1).

To obtain a more detailed thermodynamic description of residue contributions to the binding free energy, the ΔG_{bind} value was decomposed to each residue and the corresponding results were presented in Fig. 7, in which the interactions included the contributions from the residues. On the basis of the individual residue contribution to the interaction energy, several hot residues contributing to the ligand binding were identified. The hotspot residues include V122, G123, L125, Y128, Y162, I182, K185, Q186, V189, T190, T193 and K194. The polar and nonpoalr contributions of identified key residues were calculated (Fig. 7b). By comparing the binding poses of compound **3253-0207** and promazine, it can be seen that two molecules bound to prion at the same binding pocket composed of residues from β1, β2 and α2 (Fig. 8). The aromatic ring of **3253-0207** overlapped well with the tricyclic moiety of promazine. The benzimidazole fragment of **3253-0207** interacted with residues from C-terminal of H2 such as T190, T191, T193 and K194. The hotspot residues Y128, Y162, Q186, and T190 [19] having interaction with **3253-0207** were consistent with the residues involved in the interaction with promazine.

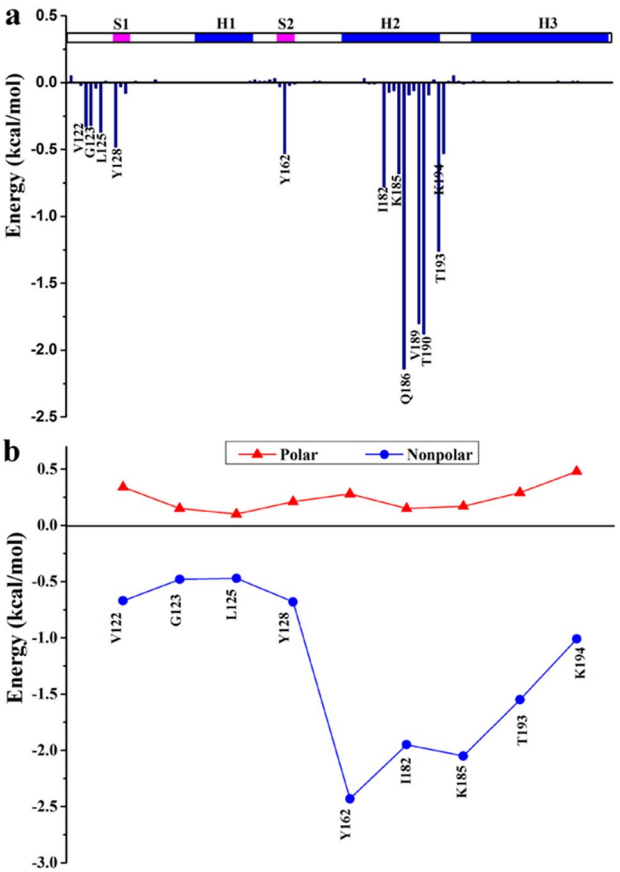

Fig. 7 Energy contributions of prion protein to ligand binding. **a** Intermolecular ligand-receptor per-residue interaction spectrum of the complex. **b** Polar (red) and nonpolar (blue) interaction energy of the complex

Most of the previously studied molecules are polymers such as pentosan polysulfate, dextran sulfate, HPA-23 and dentritic polyamines. These structures are not suitable to perform molecular docking study. The inhibiting activities of these molecules are primarily due to prevention of new PrP^{Sc} accumulation rather than stabilization of PrP^C [61, 62]. To investigate the possible mechanism of action of other small molecules such as Suramin, Congo Red and Quinacrine, a molecular docking analysis was carried out based on the binding pocket used in this workflow. Unfortunately, Suramin cannot bind to the Promazine binding pocket due to its large size. The other two molecules Congo Red and Quinacrine were docked to the binding pocket with low binding affinities. Their docking scores were −3.88 and −3.75 kcal/mol for Congo Red and Quinacrine, respectively.

Table 1 Calculated binding free energy and its components (kcal/mol) based on MM–GBSA method for the complex

Components	ΔE_{ele}	ΔE_{vdw}	ΔE_{MM}	ΔG_{sol-np}	$\Delta G_{sol-ele}$	ΔG_{sol}	ΔG_{polar}	$\Delta G_{nonpolar}$	ΔG_{bind}
Energies	−5.01	−26.98	−31.99	−4.35	13.75	9.41	8.74	−31.33	−22.59

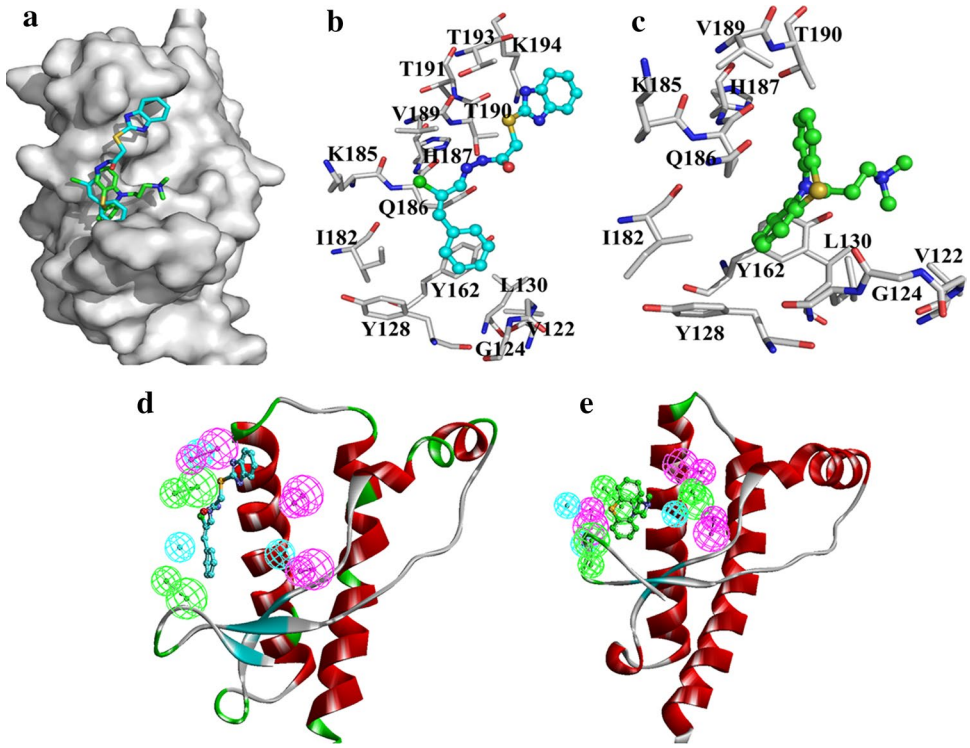

Fig. 8 Compound **3253-0207** and promazine at the binding sites of prion protein. **a** Surface representation of the binding sites with the ligands shown in sticks. **b** The interactions between compound **3253-0207** and prion. **c** The interactions between promazine and prion. **d**, **e** Are constructed pharmacophore models based on the complex of PrP-**3253-0207** and PrP-promazine (hydrophobic, acceptor and donor features are colored cyan, green and magenta, respectively)

When aligned with the crystal Promazine, it can be seen that Congo Red partially overlapped with Promazine, while Quinacrine bound in the pocket near that of Promazine (Fig. S4). These docking results proved that the mechanism of action of Congo Red and Quinacrine are different from the inhibitors discovered in our work.

Conclusions

In this work, we identified five compounds that could interact and bind with mouse prion protein (117–231) with micromolar affinity using fluorescence quenching assay. Subsequently, via surface plasmon resonance approach, compound **3253-0207** was confirmed to be a potent prion binder with binding K_D of about 26 μM. ThT fluroescence assay further proved the inhibition effect of this compound on prion amyloid formation. Molecular dynamics simulation indicated that compound **3253-0207** can bind to a pocket composed of residues from β1, β2 and α2. The hotspot residues involved in **3253-0207** binding are mainly hydrophobic. Compound **3253-0207** could interact and bind with the monomeric prion protein and further interrupt fibril formation.

Acknowledgements This work was supported by the National Nature Science Foundation of China (Grant No. 21675070) and the Fundamental Research Funds for the Central Universities (Grant No. lzujbky-2016-146).

References

1. Collinge J, Sidle KC, Meads J, Ironside J, Hill AF (1996) Nature 383:685–690
2. Heinemann U, Krasnianski A, Meissner B, Varges D, Kallenberg K, Schulz-Schaeffer W, Steinhoff B, Grasbon-Frodl E, Kretzschmar H, Zerr I (2007) Brain 130(5):1350–1359
3. Prusiner SB (1998) Proc Natl Acad Sci USA 95(23):13363–13383
4. Collinge J (2001) Annu Rev Neurosci 24(1):519–550
5. Stahl N, Baldwin MA, Teplow DB, Hood L, Gibson BW, Burlingame AL, Prusiner SB (1993) Biochemistry 32(8):1991–2002
6. Sigurdson CJ, Nilsson KPR, Hornemann S, Heikenwalder M, Manco G, Schwarz P, Ott D, Rülicke T, Liberski PP, Julius C (2009) Proc Natl Acad Sci USA 106(1):304–309
7. Castilla J, Saá P, Hetz C, Soto C (2005) Cell 121(2):195–206
8. Pan K-M, Baldwin M, Nguyen J, Gasset M, Serban A, Groth D, Mehlhorn I, Huang Z, Fletterick RJ, Cohen FE (1993) Proc Natl Acad Sci USA 90(23):1096210966
9. Caughey BW, Dong A, Bhat KS, Ernst D, Hayes SF, Caughey WS (1991) Biochemistry 30(31):7672–7680
10. Prusiner SB (1991) Science 252(5012):1515–1522
11. Trevitt CR, Collinge J (2006) Brain 129(Pt 9):2241–2265
12. Poncet-Montange G, St Martin SJ, Bogatova OV, Prusiner SB, Shoichet BK, Ghaemmaghami S (2011) J Biol Chem 286(31):27718–27728
13. Ghaemmaghami S, May BC, Renslo AR, Prusiner SB (2010) J Virol 84(7):3408–3412
14. Bertsch U, Winklhofer KF, Hirschberger T, Bieschke J, Weber P, Hartl FU, Tavan P, Tatzelt J, Kretzschmar HA, Giese A (2005) J Virol 79(12):7785–7791
15. Giese A, Kretzschmar H (2001) Prion-induced neuronal damage—the mechanisms of neuronal destruction in the subacute spongiform encephalopathies. The mechanisms of neuronal damage in virus infections of the nervous system. Springer, Berlin, pp 203–217

16. Antonyuk SV, Trevitt CR, Strange RW, Jackson GS, Sangar D, Batchelor M, Cooper S, Fraser C, Jones S, Georgiou T, Khalili-Shirazi A, Clarke AR, Hasnain SS, Collinge J (2009) Proc Natl Acad Sci USA 106(8):25542558
17. Singh J, Udgaonkar JB (2015) Angew Chem Int Ed Engl 54(26):7529–7533
18. Ghaemmaghami S, Russo M, Renslo AR (2014) J Med Chem 57(16):6919–6929
19. Baral PK, Swayampakula M, Rout MK, Kav NN, Spyracopoulos L, Aguzzi A, James MN (2014) Structure 22(2):291–303
20. Singh J, Kumar H, Sabareesan AT, Udgaonkar JB (2014) J Am Chem Soc 136(48):16704–16707
21. Rester U (2008) Curr Opin Drug Discov Dev 11(4):559–568
22. Walters WP, Stahl MT, Murcko MA (1998) Drug Discov Today 3(4):160–178
23. Lakowicz JR (1983) Quenching of fluorescence. Principles of fluorescence spectroscopy. Springer, New York, pp 277–330
24. Mátyus L, Szöllősi J, Jenei A (2006) J Photochem Photobiol B 83(3):223–236
25. Rich RL, Myszka DG (2003) J Mol Recognit 16(6):351–382
26. Rich RL, Hoth LR, Geoghegan KF, Brown TA, LeMotte PK, Simons SP, Hensley P, Myszka DG (2002) Proc Natl Acad Sci USA 99(13):8562–8567
27. Navratilova I, Hopkins AL (2010) ACS Med Chem Lett 1(1):44–48
28. Zhou T, Xu L, Dey B, Hessell AJ, Van Ryk D, Xiang S-H, Yang X, Zhang M-Y, Zwick MB, Arthos J (2007) Nature 445(7129):732–737
29. Biancalana M, Makabe K, Koide A, Koide S (2009) J Mol Biol 385(4):1052–1063
30. Luchsinger JA, Tang M, Siddiqui M, Shea S, Mayeux R (2004) J Am Geriatr Soc 52(4):540–546
31. Xue W, Pan D, Yang Y, Liu H, Yao X (2012) Antiviral Res 93(1):126–137
32. Dodson GG, Lane DP, Verma CS (2008) EMBO Rep 9(2):144–150
33. Dror RO, Dirks RM, Grossman JP, Xu H, Shaw DE (2012) Annu Rev Biophys 41:429–452
34. Kaminski GA, Friesner RA, Tirado-Rives J, Jorgensen WL (2001) J Phys Chem B 105(28):6474–6487
35. Friesner RA, Banks JL, Murphy RB, Halgren TA, Klicic JJ, Mainz DT, Prpasky MP, Knoll EH, Sheelley M, Perry JK, Shaw DE, Francis P, Shenkin PS (2004) J Med Chem 47:1739–1749
36. Cross JB, Thompson DC, Rai BK, Baber JC, Fan KY, Hu Y, Humblet C (2009) J Chem Inf Model 49(6):1455–1474
37. Bjorndahl TC, Zhou GP, Liu X, Perez-Pineiro R, Semenchenko V, Saleem F, Acharya S, Bujold A, Sobsey CA, Wishart DS (2011) Biochemistry 50(7):1162–1173
38. Yin S-M, Zheng Y, Tien P (2003) Protein Expr Purif 32(1):104–109
39. Bradford MM (1976) Anal Biochem 72(1–2):248–254
40. Lakowicz JR, Weber G (1973) Biochemistry 12(21):4161–4170
41. Mehra J, Rechenberg H (2001) The historical development of quantum theory. Volume 1 part 1 the quantum theory of Planck, Einstein, Bohr and Sommerfeld 1900–1925: its foundation and the rise of its difficulties. Springer, New York, pp 1900–1925
42. Frostell-Karlsson Å, Remaeus A, Roos H, Andersson K, Borg P, Hämäläinen M, Karlsson R (2000) J Med Chem 43(10):1986–1992
43. Feltis B, Sexton B, Glenn F, Best M, Wilkins M, Davis T (2008) Biosens Bioelectron 23(7):1131–1136
44. Bocharova OV, Breydo L, Parfenov AS, Salnikov VV, Baskakov IV (2005) J Mol Biol 346(2):645–659
45. Baskakov IV (2004) J Biol Chem 279(9):7671–7677
46. Case DA, Cheatham TE, Darden T, Gohlke H, Luo R, Merz KM, Onufriev A, Simmerling C, Wang B, Woods RJ (2005) J Comput Chem 26(16):1668–1688
47. Frisch MJ, Trucks GW, Schlegel HB, Scuseria GE, Robb MA, Cheeseman JR, Scalmani G, Barone V, Mennucci B, Petersson GA, Nakatsuji H, Caricato M, Li X, Hratchian HP, Izmaylov AF, Bloino J, Zheng G, Sonnenberg JL, Hada M, Ehara M, Toyota K, Fukuda R, Hasegawa J, Ishida M, Nakajima T, Honda Y, Kitao O, Nakai H, Vreven T, Montgomery JJA, Peralta JE, Ogliaro F, Bearpark M, Heyd JJ, Brothers E, Kudin KN, Staroverov VN, Kobayashi R, Normand J, Raghavachari K, Rendell A, Burant JC, Iyengar SS, Tomasi J, Cossi M, Rega N, Millam NJ, Klene M, Knox JE, Cross JB, Bakken V, Adamo C, Jaramillo J, Gomperts R, Stratmann RE, Yazyev O, Austin AJ, Cammi R, Pomelli C, Ochterski JW, Martin RL, Morokuma K, Zakrzewski VG, Voth GA, Salvador P, Dannenberg JJ, Dapprich S, Daniels AD, Farkas Ö, Foresman JB, Ortiz JV, Cioslowski J, Fox DJ (2009) Gaussian 09. Gaussian, Inc., Wallingford
48. Fox T, Kollman PA (1998) J Phys Chem B 102(41):8070–8079
49. Bayly CI, Cieplak P, Cornell W, Kollman PA (1993) J Phys Chem 97(40):10269–10280
50. Wang J, Wolf RM, Caldwell JW, Kollman PA, Case DA (2004) J Comput Chem 25(9):1157–1174
51. Lindorff-Larsen K, Piana S, Palmo K, Maragakis P, Klepeis JL, Dror RO, Shaw DE (2010) Proteins 78(8):1950–1958
52. Onufriev A, Bashford D, Case DA (2000) J Phys Chem B 104(15):3712–3720
53. Tsui V, Case DA (2000) Biopolymers 56(4):275–291
54. Massova I, Kollman PA (2000) Perspect Drug Discov 18(1):113–135
55. Sitkoff D, Sharp KA, Honig B (1994) J Phys Chem 98(7):1978–1988
56. Pearlman DA, Case DA, Caldwell JW, Ross WS, Cheatham TE, DeBolt S, Ferguson D, Seibel G, Kollman P (1995) Comput Phys Commun 91(1):1–41
57. Baell JB, Holloway GA (2010) J Med Chem 53(7):2719–2740
58. Rolinski OJ, Amaro M, Birch DJ (2010) Biosens Bioelectron 25(10):2249–2252
59. Zhou Z, Yan X, Pan K, Chen J, Xie ZS, Xiao GF, Yang FQ, Liang Y (2011) Biophys J 101(6):1483–1492
60. Zhou Z, Fan JB, Zhu HL, Shewmaker F, Yan X, Chen X, Chen J, Xiao GF, Guo L, Liang Y (2009) J Biol Chem 284(44):30148–30158
61. Caughey B, Raymond GJ (1993) J Virol 67(2):643–650
62. Raymond GJ, Olsen EA, Lee KS, Raymond LD, Bryant PK, Baron GS, Caughey WS, Kocisko DA, McHolland LE, Favara C, Langeveld J, Zijiderveld F, Mayer RT, Miller MW, Williams ES, Caughery B (2006) J Virol 80(2):596–604